Supplementary materials

Text S1 Generation process of improved 3D discrete failure mechanism

The generation process of the improved 3D discrete failure mechanism could be divided into four parts. Figure S1 presents the generation process of discrete boundary *AF* and *BF*.

(1) Construction of discretized boundary *BF*

P_i and P_{i+1} are adjacent points on the discrete boundary *BF*, which is shaped by connecting a series of line segments P_iP_{i+1} (i=1, 2, 3, …, n). The coordinates of the rotation center *O* of improved discrete failure mechanism are expressed as:

$$\begin{cases} y_{\mathrm{o}} = r_{\mathrm{E}} \cdot \cos\beta_{\mathrm{E}} - D/2 \\ z_{\mathrm{o}} = r_{\mathrm{E}} \cdot \sin\beta_{\mathrm{E}} \end{cases} \tag{1}$$

In Figure S1(a), the unit normal vector $\boldsymbol{v_i}=(y_{vi}, z_{vi})$ of $\boldsymbol{P_iO}$ at P_i is given as:

$$\begin{cases} y_{vi} = -\sin\beta_i \\ z_{vi} = -\cos\beta_i \end{cases} \tag{2}$$

$\boldsymbol{n_i}=(y_{ni}, z_{ni})$ is the unit normal vector of boundary curve $\boldsymbol{P_iP_{i+1}}$. The angle between the vectors $\boldsymbol{v_i}$ and $\boldsymbol{n_i}$ is $\pi/2+\varphi_i$ [1]. Thus, the vector $\boldsymbol{n_i}$ can be formulated as:

$$\begin{cases} y_{ni} = -\cos(\beta_i + \varphi_i) \\ z_{ni} = \sin(\beta_i + \varphi_i) \end{cases} \tag{3}$$

Since $\overline{\boldsymbol{P_iP_{i+1}}}=\overline{\boldsymbol{P_iO}}+\overline{\boldsymbol{OP}}_{\boldsymbol{i+1}}$ and $\boldsymbol{n_i}\cdot\boldsymbol{P_iP_{i+1}}=0$, the following equation is obtained by introducing unit vector $\boldsymbol{\omega_{i+1}}=(y_{\omega_{i+1}}, z_{\omega_{i+1}})$ and length λ_{i+1} of $\boldsymbol{OP_{i+1}}$ as:

$$\boldsymbol{n_i} \cdot \left(\boldsymbol{P_iO} + \lambda_{i+1}\boldsymbol{\varpi}_{i+1}\right) = 0 \tag{4}$$

with

$$\begin{cases} y_{\varpi_{i+1}} = -\cos\beta_{i+1} \\ z_{\varpi_{i+1}} = \sin\beta_{i+1} \end{cases} \tag{5}$$

where β_{i+1} is equal to $\beta_i+\varpi_\beta$. Combining Eqs. (1)–(5), the length λ_{i+1} can be obtained as:

$$\lambda_{i+1} = \frac{\left(y_{\mathrm{o}} - y_i\right)\cdot\cos\left(\beta_i + \varphi_i\right) - \left(z_{\mathrm{o}} - z_i\right)\cdot\sin\left(\beta_i + \varphi_i\right)}{\cos\left(\beta_i + \varphi_i\right)\cdot\cos\beta_{i+1} + \sin\left(\beta_i + \varphi_i\right)\cdot\sin\beta_{i+1}} \tag{6}$$

Thus, the coordinates of the point P_{i+1} on discretized boundary *BF* are obtained as

$$\begin{cases} y_{i+1} = y_{\mathrm{o}} - \lambda_{i+1}\cos\beta_{i+1} \\ z_{i+1} = z_{\mathrm{o}} + \lambda_{i+1}\sin\beta_{i+1} \end{cases} \tag{7}$$

(2) Construction of discretized boundary *AF*

In Figure S1(b), the unit normal vector $\boldsymbol{v_j}=(y_{vj}, z_{vj})$ of $\boldsymbol{P_jO}$ at point P_j is expressed as:

$$\begin{cases} y_{vj} = -\sin\beta_j \\ z_{vj} = -\cos\beta_j \end{cases} \tag{8}$$

$n_j = (y_{nj}, z_{nj})$ is unit normal vector of boundary curve P_jP_{j+1}, the angle between v_j and n_j is $\pi/2+\varphi_j$ [1]. Thus, the vector n_j can be formulated as:

$$\begin{cases} y_{nj} = -\cos(\beta_j - \varphi_j) \\ z_{nj} = -\sin(\beta_j - \varphi_j) \end{cases} \tag{9}$$

Combining Eqs. (4)−(5) and (8)−(9), the length λ_{i+1} is obtained as

$$\lambda_{j+1} = \frac{\left(y_o - y_j\right)\cdot\cos\left(\varphi_j - \beta_j\right) + \left(z_o - z_j\right)\cdot\sin\left(\varphi_j - \beta_j\right)}{\cos\left(\varphi_j - \beta_j\right)\cdot\cos\beta_{j+1} - \sin\left(\varphi_j - \beta_j\right)\cdot\sin\beta_{j+1}} \tag{10}$$

Then, the coordinates of point P_{i+1} on discretized boundary BF are obtained as:

$$\begin{cases} y_{j+1} = y_o - \lambda_{j+1}\cos\beta_{j+1} \\ z_{j+1} = z_o + \lambda_{j+1}\sin\beta_{j+1} \end{cases} \tag{11}$$

(3) Construction of point F

The termination condition for generating discrete points on boundaries AF and BF from points A and B is that z_{j+1} is greater than z_{i+1}. Based on linear interpolation method, the final generation point F is formulated as,

$$\begin{cases} y_F = y_j + \dfrac{\left(z_i - z_j\right)\cdot\left(y_{i+1} - y_i\right)\cdot\left(y_{j+1} - y_j\right)}{\left(y_{i+1} - y_i\right)\cdot\left(z_{j+1} - z_j\right) - \left(y_{j+1} - y_j\right)\cdot\left(z_{i+1} - z_i\right)} \\ z_F = \dfrac{z_i\cdot\left(y_{i+1} - y_i\right)\cdot\left(z_{j+1} - z_j\right) - z_j\cdot\left(y_{j+1} - y_j\right)\cdot\left(z_{i+1} - z_i\right)}{\left(y_{i+1} - y_i\right)\cdot\left(z_{j+1} - z_j\right) - \left(y_{j+1} - y_j\right)\cdot\left(z_{i+1} - z_i\right)} \end{cases} \tag{12}$$

(4) Generation of 3D failure surface

The process of generating 3D failure surface of improved discrete failure mechanism is concluded three steps in:

Step 1: The circular tunnel face is divided into $2N$ points symmetrically along Y axis by discretization technique. Then, the failure boundaries are divided into Section 1 ($\beta_B \le \beta_j < \beta_A$) and Section 2 ($\beta_A \le \beta_j \le \beta_F$). β_j is the rotation angle of point P_i at the failure mechanism.

Step 2: The Section 1 is divided into N planes passing through rotation center O and two symmetrically discretized points A_m and A'_m (The Section 2 is subdivided in several planes passing through the point O with a constant angle of δ_B between adjacent planes).

Step 3: Using the 3D "point by point" strategy [2], the new point $P_{i,j+1}$ on later plane Ψ_{j+1} is produced from points $P_{i,j}$, $P_{i+1,j}$ on last plane Ψ_j (see Figure S3). Finally, the 3D improved discrete failure mechanism is obtained by connecting each adjacent discrete points $P_{i,j}$, $P_{i+1,j}$ and $P_{i,j+1}$.

Text S2 The sparse polynomial chaos expansion method

Assuming that the computational model ϑ involves input parameters represented as independent random variables forming an input vector $\boldsymbol{\xi}=\{\xi_1; \xi_2; \ldots, \xi_L\}$, with L denoting the quantity of input parameters. The system response Y is characterized using the PCE method as [3]:

$$Y = \vartheta(\boldsymbol{\xi}) \cong \sum_{j=1}^{P} \kappa_j \psi_{\boldsymbol{\alpha}}(\boldsymbol{\xi}) \tag{13}$$

where $\psi_\alpha(\xi)=\Pi_{j=1}^{L} H_{\alpha i}(\xi_i)$ denotes the multivariate polynomials; $H_{\alpha i}(\xi_i)$ denotes the univariate polynomial; $\boldsymbol{\alpha}=(\alpha_1, ..., \alpha_i, \ldots, \alpha_L)$ denotes a L-dimensional vector containing a series of integers α_i; α_i denotes the degree of univariate polynomial; κ_j denotes the unknown coefficients of PCE; P denotes term number in truncated SPCE. Compared with traditional PCE method, BLATMAN et al [4] introduced the hyperbolic truncation scheme to improve computational performance of surrogate model by shorting number of PCE terms. The hyperbolic truncation scheme is determined by specifying q-quasi-norm of $\boldsymbol{\alpha}$ as:

$$\|\boldsymbol{\alpha}\|_q = \left(\sum_{i=1}^{L} \alpha_i^q\right)^{\frac{1}{q}},\ 0 < q < 1 \tag{14}$$

The q-quasi-norm of $\boldsymbol{\alpha}$ does not exceed p. The recommended range of 0.7−0.9 for q can strike an appropriate balance between accuracy and sparsity, as suggested by BLATMAN et al [4].

To further reduce PCE terms that contribute less to the accuracy of the model and extract prominent terms from the candidate basis obtained by hyperbolic truncation scheme, the stepwise regression technique [5] and least angle regression technique [4] were applied in this study. The SPCE procedure involves four user-specified indices: maximum degree of sparse polynomial $p_{\max}$, norm parameter q, the SPCE target accuracy Q^2_{tgt}, and cut-off value ε_{cut}. The detailed parameter definition ($p_{\max}$, Q^2_{tgt}, ε_{cut}) and calculation in SPCE method can refer to BLATMAN et al [4] and YANG et al [6]. In this work, the four indices are initialized as follows: target accuracy Q^2_{tgt} is 0.999, cut-off value ε_{cut} is 5×10^{-5}, maximum degree $p_{\max}$ is 5, and norm parameter q is 0.8.

Table S1 Values of random and deterministic parameters

Parameter	Random variable						
	c/kPa	φ/(°)	k_h	V_s/(m·s^{-1})	T/s	γ/(kN·m^{-3})	σ_U/kPa
Mean (μ)	10	15	0.2	150	0.1	18	—
COV/%	20	10	25	10	10	5	15
Parameter	Deterministic parameter						
	C/m	D/m	λ_c	λ_φ	ξ	k_v	V_p/(m·s^{-1})
Mean (μ)	10	10	1	1	0.1	0.1	280.5
COV/%	0	0	0	0	0	0	0

Table S2 Engineering case parameters of the sandstone soils

c/kPa	φ/(°)	γ/(kN·m^{-3})	C/m	D/m	V_s/(m·s^{-1})	ξ
0	40	21	15	12.4	400	0.15

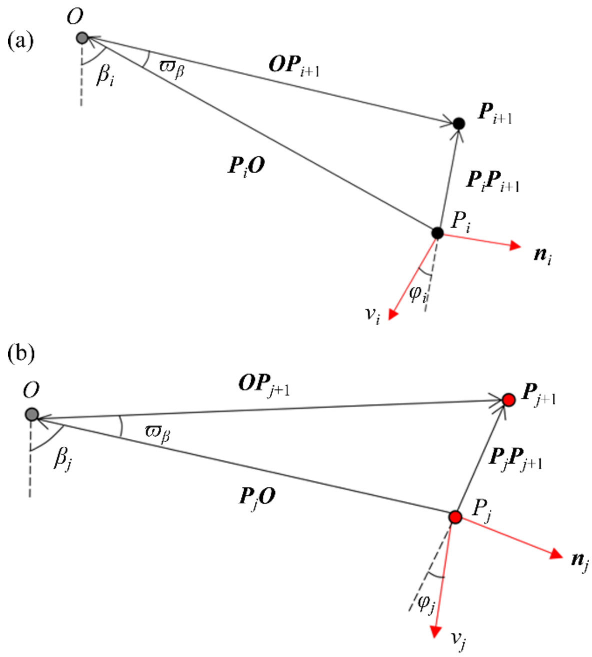

Figure S1 Generation of the discrete points: (a) Point P_{i+1} on BF; (b) Point P_{j+1} on AF

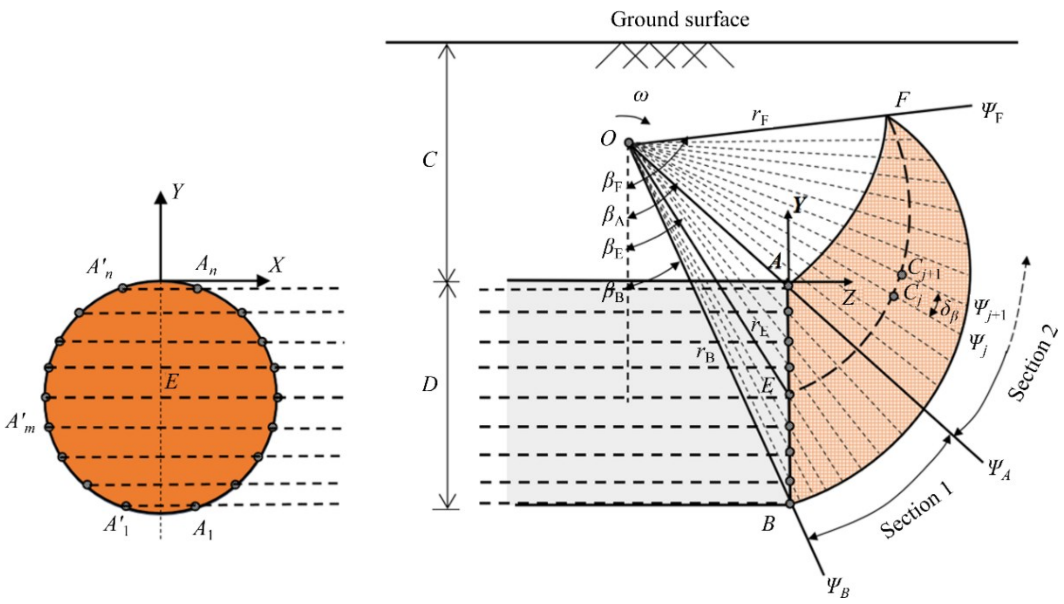

Figure S2 Improved discrete failure mechanism in horizontal and longitudinal planes

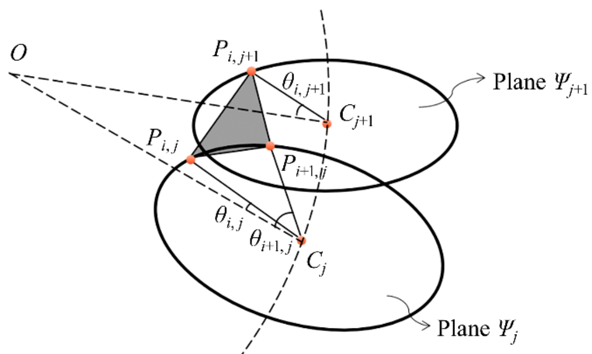

Figure S3 Point generation diagram between two adjacent planes with "point by point" strategy

References

[1] CHEN W F, SNITBHAN N, FANG H Y. Stability of slopes in anisotropic, nonhomogeneous soils [J]. Canadian Geotechnical Journal, 1975, 12(1): 146−152. DOI: 10.1139/t75-014.

[2] MOLLON G, DIAS D, SOUBRA A H. Rotational failure mechanisms for the face stability analysis of tunnels driven by a pressurized shield [J]. International Journal for Numerical and Analytical Methods in Geomechanics, 2011, 35(12): 1363−1388. DOI: 10.1002/nag.962.

[3] SUDRET B. Global sensitivity analysis using polynomial chaos expansions [J]. Reliability Engineering & System Safety, 2008, 93(7): 964−979. DOI: 10.1016/j.ress.2007.04.002.

[4] BLATMAN G, SUDRET B. Adaptive sparse polynomial chaos expansion based on least angle regression [J]. Journal of Computational Physics, 2011, 230(6): 2345−2367. DOI: 10.1016/j.jcp.2010.12.021.

[5] BLATMAN G, SUDRET B. Efficient computation of global sensitivity indices using sparse polynomial chaos expansions [J]. Reliability Engineering & System Safety, 2010, 95(11): 1216−1229. DOI: 10.1016/j.ress.2010.06.015.

[6] YANG Tao, ZOU Jin-feng, PAN Qiu-jing. A sequential sparse polynomial chaos expansion using Voronoi exploration and local linear approximation exploitation for slope reliability analysis [J]. Computers and Geotechnics, 2021, 133: 104059. DOI: 10.1016/j.compgeo.2021.104059.